Supplemental Information
Defining Organelle Remodeling During Infection Reveals Key Translocations for Herpesvirus Production

CONTENTS

SUPPLEMENTAL FIGURES

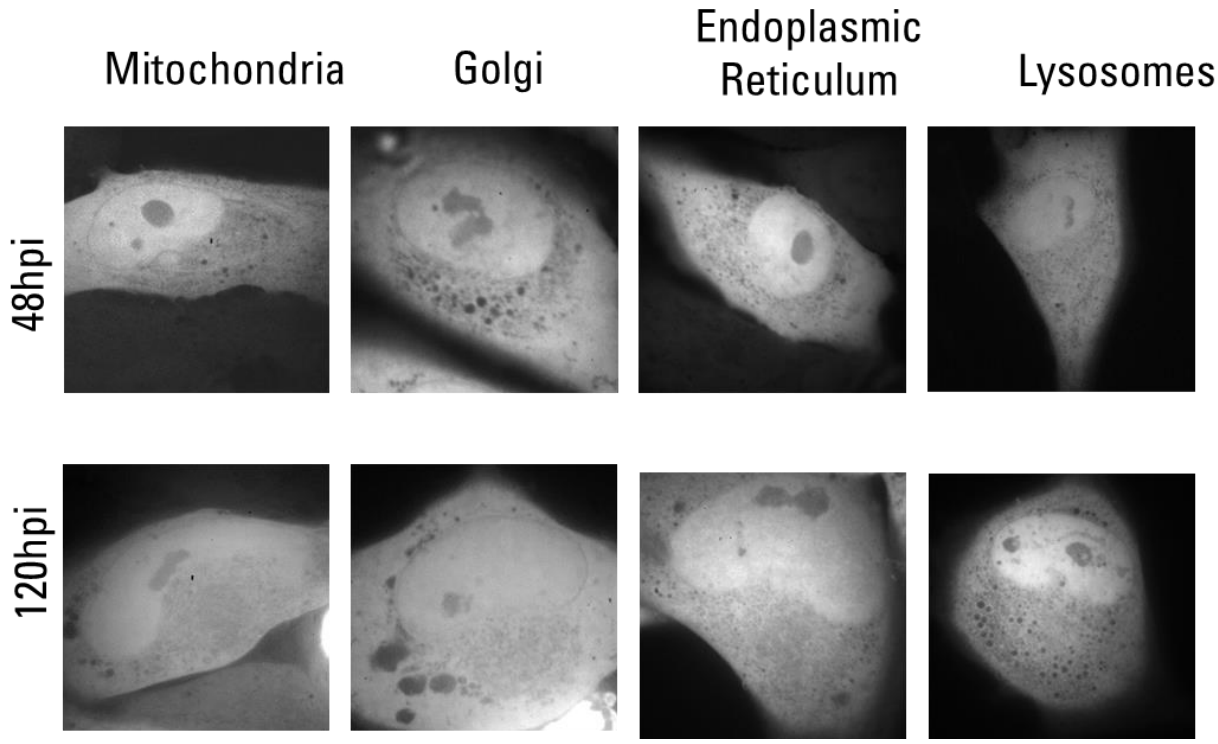

Figure S1. Expression of GFP as a marker for infection. Related to Fig 1

Green fluorescent protein (GFP) expression confirms viral infection of the cells shown in figure 1.

Movie S1. Organelle dynamics throughout HCMV infection. Related to Fig 1

Representative time lapse movies of mitochondria (30sec), endoplasmic reticulum (15sec), Golgi complex (15sec), and lysosomes (15sec), showing the mobility of organelles in uninfected cells and infected cells at 48 and 120 hpi. Each organelle/time point is shown twice at 3.5X speed.

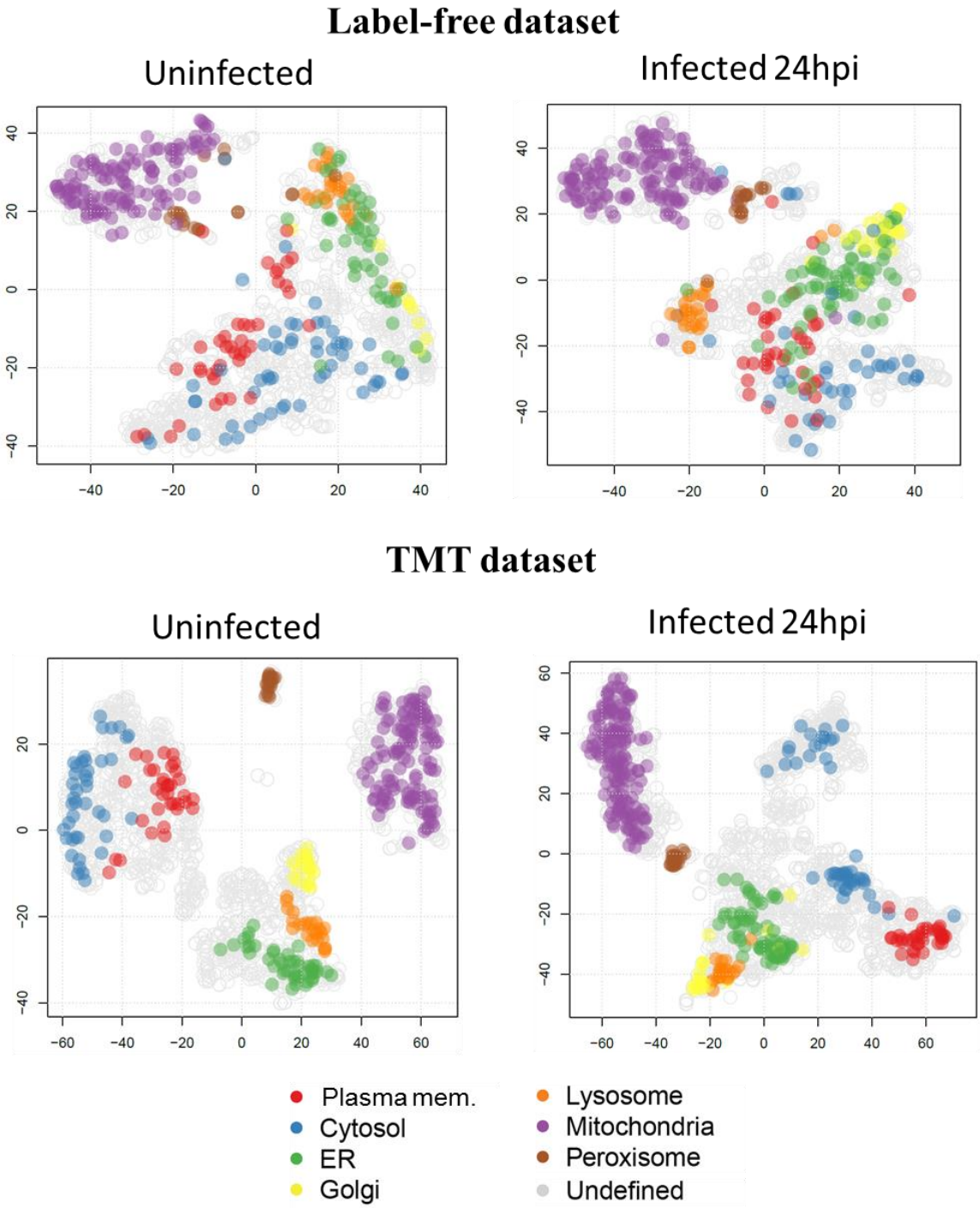

Figure S2. Quality assessment of dataset and organelle markers for the assignment of protein subcellular localization. Related to Fig 2.

Protein abundance across six organelle fractions represented in two dimensional space. Markers for each subcellular organelle are shown in color. Partial separation between organelle clusters is observed in the label-free dataset (top), while distinct clusters were readily observed in the TMT dataset (bottom).

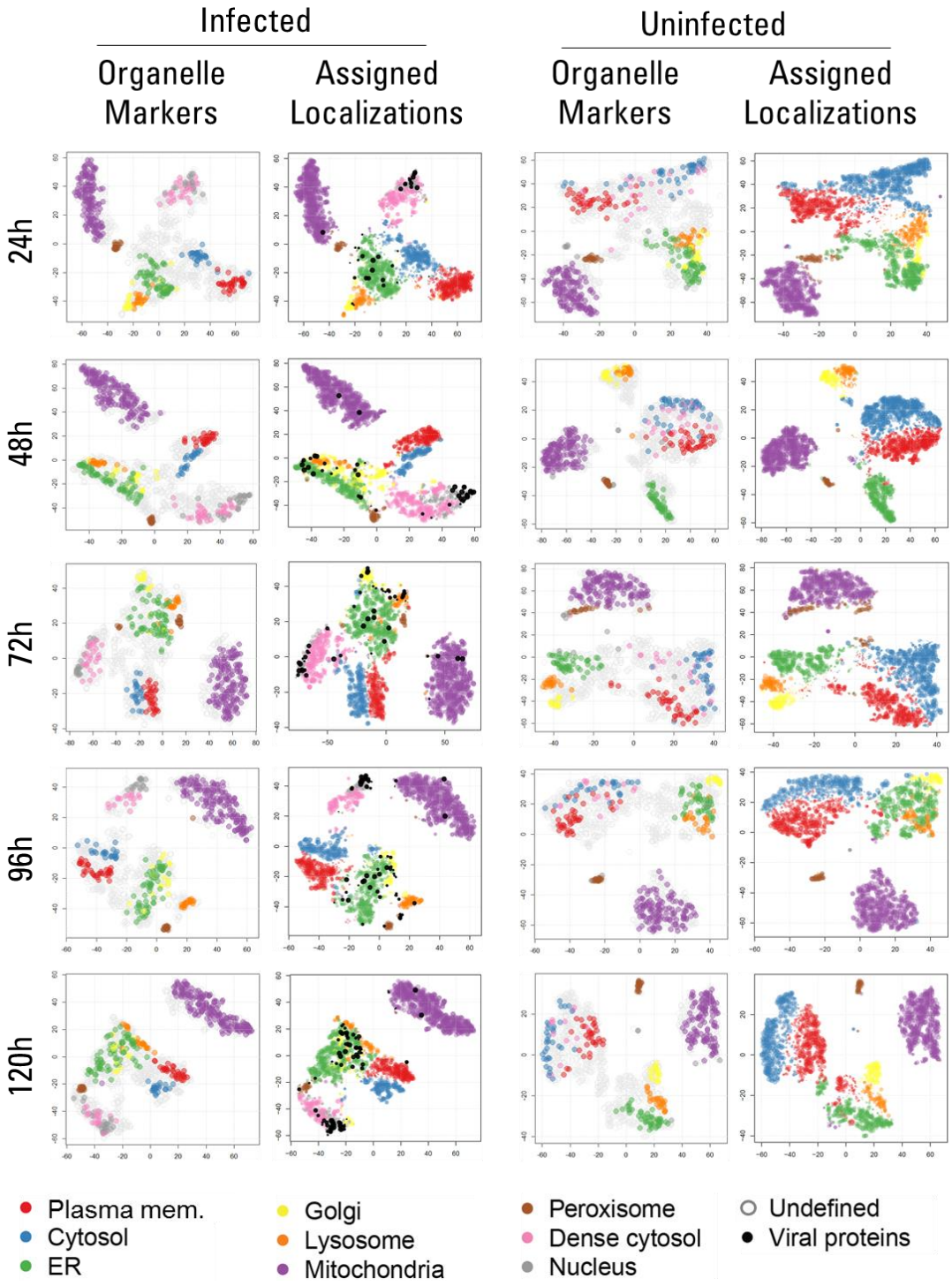

Figure S3. Data structure of TMT datasets collected by organelle fractionation of infected and uninfected cells. Related to Fig 4

Visualization of fractionation data in 2 dimensions using t-SNE for uninfected (left) and infected (right) samples collected at 24, 48, 72, 96, and 120 hpi. The proteins are color coded either using the annotation for organelle markers or using the localizations predicted by machine learning (assigned localizations). For the assigned localizations, the size of the dots represents the probability scores from the nnet algorithm, with larger dots representing higher scores.

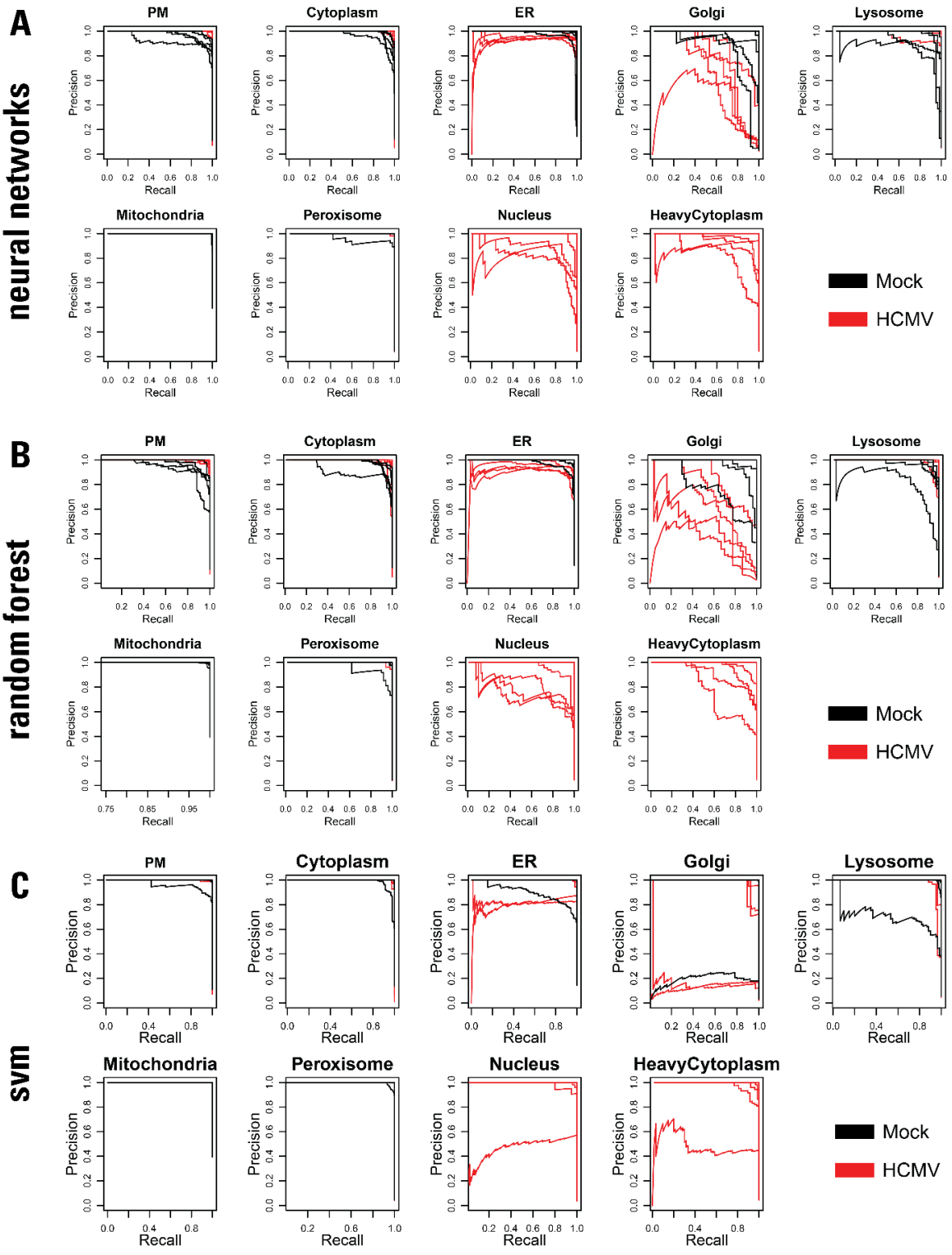

Figure S4. Accuracy assessment of machine learning methods for the categorization of proteins to subcellular organelles. Related to Fig 4.

Precision/recall curves to assess classification performance for three machine learning models: averaged neural networks, random forest, and support vector machines (svm). Each line represents a different uninfected (black) or infected (red) sample. Precission and recall was determined by leave group out cross validation over 100 iterations.

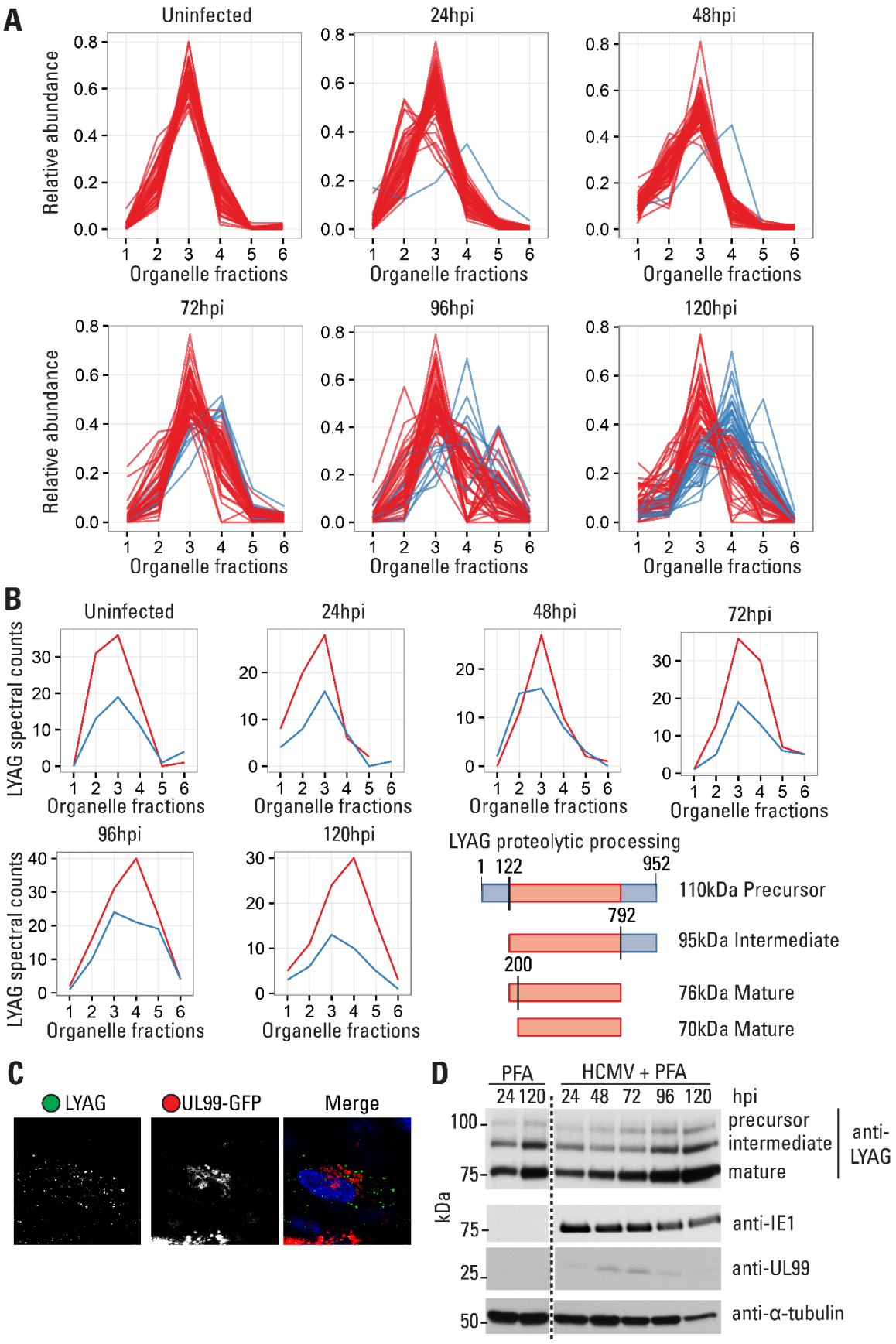
A
Uninfected
24hpi
48hpi
72hpi
96hpi
120hpi
Relative abundance
Organelle fractions
B
LYAG spectral counts
LYAG proteolytic processing
1
122
952
110kDa Precursor
792
95kDa Intermediate
200
76kDa Mature
70kDa Mature
C
LYAG
UL99-GFP
Merge
D
PFA
HCMV + PFA
24 120
24 48 72 96 120
hpi
precursor
intermediate
mature
anti-LYAG
kDa
anti-IE1
anti-UL99
anti-α-tubulin

Figure S5. Redistribution of lysosome proteins during density gradient fractionation upon infection. Related to Fig 4.

A Distribution of lysosome proteins throughout the density gradient at multiple time points of infection and in uninfected cells. Proteins with profiles that are more abundant in lighter fractions are shown in red and in denser fraction in blue.

B Distribution of LYAG spectral counts throughout the density gradient at multiple time points of infection and in uninfected cells. Spectral counts were grouped for those originating from peptides at the ends (blue) or from the 76kDa mature form (red). Model for LYAG processing (bottom-right corner) showing regions considered as ends (blue) and center (red), with the numbers stating the aminoacids at which LYAG is cleaved. A total of 17 theoretical tryptic peptides are expected from the ends of LYAG corresponding to the intermediate and precursor forms and 23 from the center region corresponding to both mature and precursors. Between all samples, we detected 47% of the end peptides and 60% of the center peptides showing good coverage of this protein.

C IF for endogenous LYAG and UL99-GFP (marker for AC) at 120hpi. LYAG does not co-localize with the marker of the assembly complex.

D WB showing the requirement of late gene expression for differential LYAG processing. Samples were collected from uninfected cells or from cells infected with HCMV and treated with PFA to inhibit late gene expression. Markers for early gene expression (IE1), late gene expression (UL99), and loading control (tubulin) are shown.

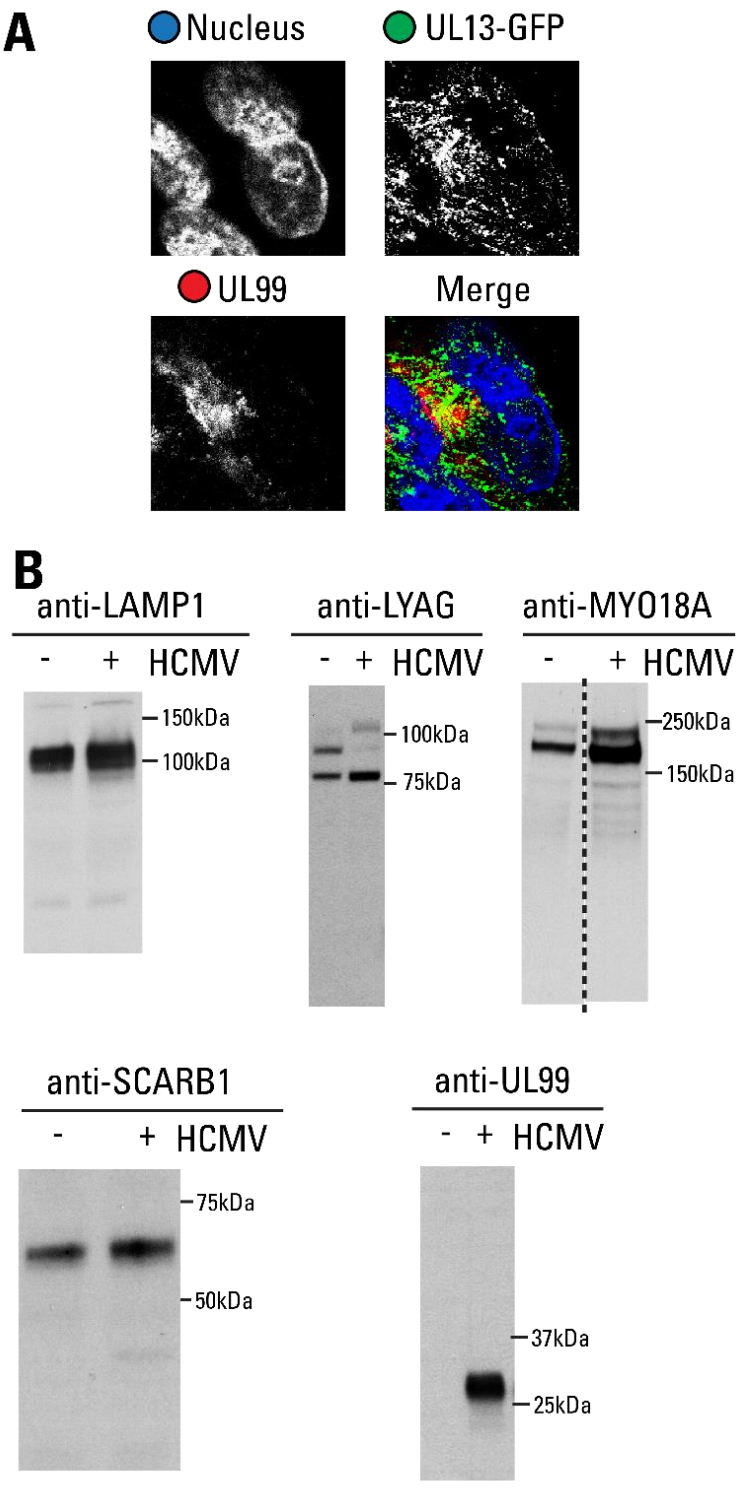

Figure S6. Co-localization of UL13-GFP with the assembly complex. Related to Fig 5.

A Microscopy showing co-localization of UL13-GFP (direct fluorescence) with UL99 (immunostaining) in fixed fibroblasts at 120hpi.

B Western blots showing specificity for antibodies used for immunofluorescence.

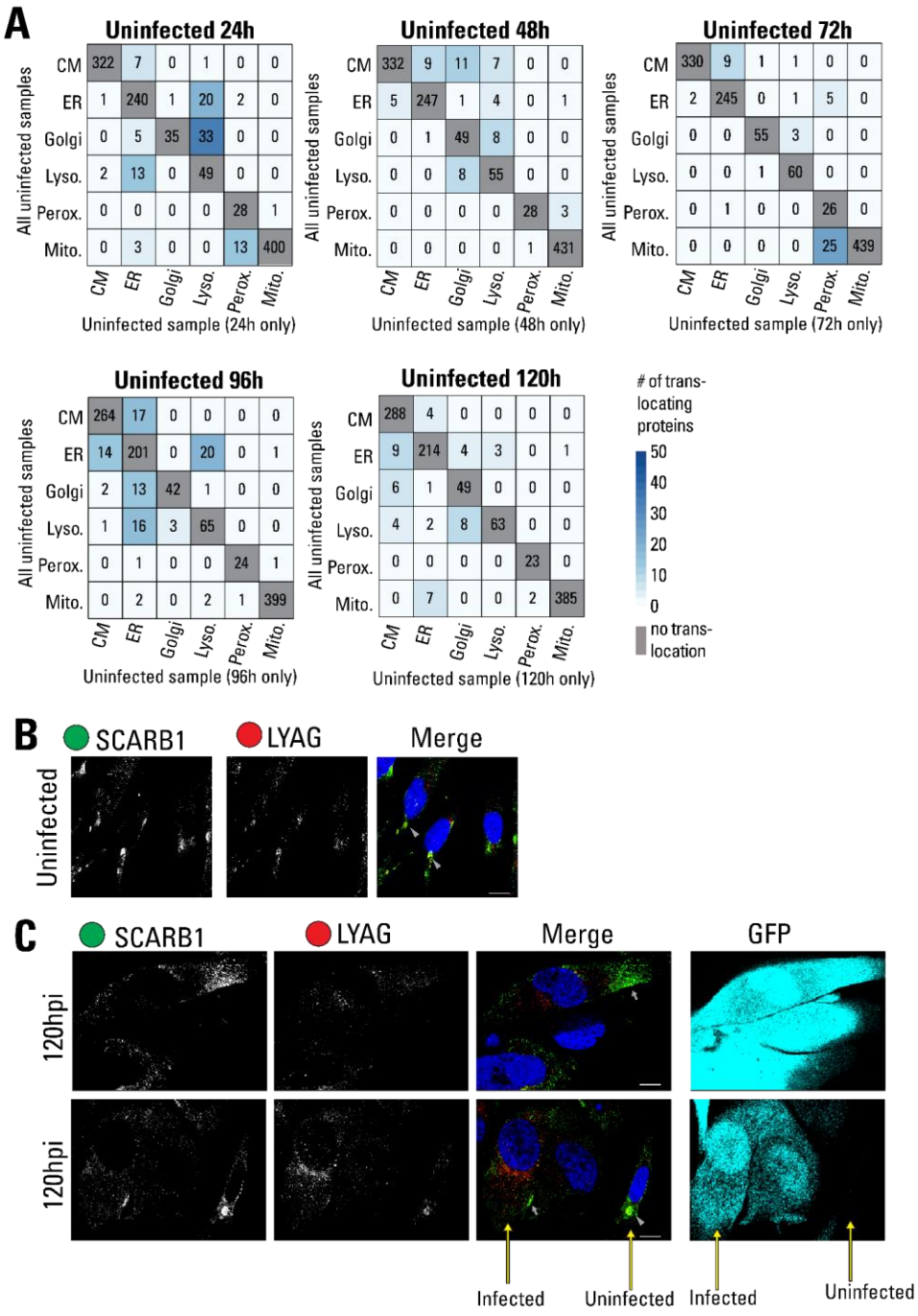

Figure S7. Translocation events between uninfected cells. Related to Fig 6.

A Heatmap showing translocation events that would be detected by comparing the predominant localization in all uninfected samples to the localization of a single uninfected sample. Rows indicate the predominant assigned localization in uninfected samples, and columns indicate the localization from a specific uninfected sample.

B Immunofluorescence images of SCARB1 (green) and LYAG (red) in uninfected cells showing their co-localization in internal vesicles (arrowheads). Nucleus is labeled in blue (Hoechst).

C Immunofluorescence images of SCARB1 (green) and LYAG (red) in cells infected with AD169 GFP, showing lack of co-localization at the cell periphery (arrows). Co-localization can be observed in the uninfected cell on the bottom row. GFP is shown as a marker of infection.

SUPPLEMENTAL TABLES IN EXCEL FORMAT

Table S1. Analysis of temporal alterations in organelle protein abundance. Related to Fig 3

(A&B) Relative protein abundance throughout HCMV infection using the label free dataset. (C) Cross-validation with dataset from Weekes et al, 2014 showing proteins up- or downregulated within each dataset. (D-I) Complete list of significant gene ontology biological process terms associated to each of the temporal clusters in Fig3A.

Table S2. Relative protein abundance across organelle fractions from the density gradient. Related to Fig 4.

Each tab shows data from the TMT dataset for each infected and uninfected time point (24, 48, 72, 96, and 120hpi).

Table S3. List of refined organelle markers used for prediction of subcellular localization. Related to Fig 4.

Table S4. Prediction and analysis of the subcellular localization of hot and viral proteins. Related to Fig 4.

(A) Grouped predicted subcellular localization for proteins identified in uninfected samples. The predominant localization is shown, along with the total prediction score for all samples, and the proportion of assignment to each organelle. (B) List of predicted subcellular localization for viral proteins throughout infection, along with the prediction score. (C) Predicted subcellular localization and prediction scores for all identified proteins in the TMT dataset. (D) Same as C, but with the bottom 25% scoring predictions for each organelle set as undefined. (E) Predicted subcellular localization and prediction scores for all identified proteins in the label-free dataset. (F) Same as E, but with the bottom 25% scoring predictions set as undefined.

Table S5. Profile of lysosome proteins and assignment to lighter or denser groups using label-free dataset from uninfected and infected samples. Related to Fig 4.

Relative abundance of lysosome proteins across the density gradient using the label-free dataset. Lysosome proteins were labeled as A if the peak of their profile was on the lighter fractions (1-3), or as B if the peak of their profiles was on the denser fractions (4-6).

Table S6. Translocation events detected for host proteins during in infection and uninfected cells. Related to Fig 6

(A) Translocation events observed using loose criteria. Primary localization in uninfected and infected samples is displayed, along with the earliest time after infection at which the translocation is observed. (B) Host proteins consistently assigned to two or more locations in uninfected cells showing their primary and secondary localization. (C) Translocation events observed using more stringent criteria. Primary localization in uninfected and infected samples is displayed, along with the earliest time after infection at which the translocation is observed.